SAND2019-14733C

High-Speed X-ray Stereo Digital Image Correlation for Fluid-Structure Interactions in a Shock Tube

Jeremy W. James[1], Elizabeth M. C. Jones[2], Enrico C. Quintana[3], Kyle P. Lynch[4], Benjamin R. Halls[2], and Justin L. Wagner[5]
Sandia National Laboratories, Albuquerque, NM 87185

X-ray stereo digital image correlation (DIC) measurements were performed at 10 kHz on a jointed structure in a shock tube at a shock Mach number of 1.42. The X-ray results were compared to optical DIC using visible light. In the X-ray measurements, an internal surface with a tantalum-epoxy DIC pattern was imaged, whereas the optical DIC imaged an external surface. The environment within the shock tube caused temperature and density gradients in the gas through which the structure was imaged, therefore leading to spatial and temporal index of refraction variations. These variations caused beam-steering effects that resulted in bias error in optical DIC measurements. X-rays were used to mitigate the effects of beam-steering caused by the shock tube environment. X-ray beam displacements were able to follow similar trends (slopes, oscillations amplitudes and frequencies) as optical beam displacements while ignoring the refraction due to shock waves. X-ray DIC also has the added advantage of being able to image internal structural responses, whereas optical DIC is only capable of measurements on the outer surface of objects.

I. Introduction

Predicting high-speed fluid-structure interactions (FSI) is difficult. One challenge is that experimental data in high-speed, compressible flows remain scarce. Some examples of high-speed FSI experiments include the structural response of a store in an aircraft bay [1], panel response under loading imposed by boundary layers [2–4], panels subjected to shock wave-boundary layer interactions [5–7], and panel response to supersonic jets. In the latter cases, attention is often given to large panel displacements, where the structural dynamics become nonlinear [6–10]. Added difficulties arise when observing jointed-structures as they are dependent on the coefficient of friction between surface and the normal loads from bolted connections [11].

The present work is part of a larger campaign at Sandia to measure the response of jointed-structures in a shock tube [11, 12]. Previous work has elucidated the nonlinear structural dynamics associated with a rocking motion of the structure induced by vortex shedding. This previous work, however, was unable to successfully measure streamwise displacements as these were largely contaminated by aero-optical distortions associated with shock waves. The present work focuses on a new method to mitigate these effects, namely X-ray digital image correlation (DIC).

DIC is a noncontact full-field displacement measurement technique [13]. The technique utilizes image sequences of the surface of the specimen. Analysis is done by segmenting frames into interrogation areas, called subsets, and the motion of the pattern between frames for each subset is calculated by minimizing a correlation criterion. Patterns are typically applied to generate high-contrast features on the surface of the object. For example, the specimen may be painted white, and then black speckles are applied. Ideally, the features should be approximately 3-5 pixels in size and the pattern needs to be random for DIC to make accurate measurements [14]. 2D-DIC uses a single camera that is perpendicular to the planar object and only captures displacements within that plane. Stereo-DIC uses two cameras to capture three-dimensional displacements on the surface of the object.

DIC is being used in a variety of experimental environments that introduce new challenges. Variations in the index of refraction in a medium is one such environment. Imaging objects in this environment cause errors when performing

[1] Student Intern, Student Member AIAA, also graduate in Mechanical Engineering at Purdue University, jerjame@sandia.gov
[2] Senior Member of the Technical Staff, Engineering Sciences Center, emjones@sandia.gov
[3] Principal Member of the Technical Staff, Engineering Sciences Center.
[4] Senior Member of the Technical Staff, Engineering Sciences Center, Member AIAA, klynch@sandia.gov.
[5] Principal Member of the Technical Staff, Engineering Sciences Center, Senior Member AIAA, jwagner@sandia.gov.

DIC using visible light, namely 'optical DIC.' The refraction variation manipulates the visible light as it travels from the object to the camera sensor. This is known as beam-steering and is a source of the DIC displacement bias error. Some examples of beam-steering include imaging through heat haze [15] and imaging through shock waves [11, 12, 15]. Both of these examples show that changes in the optical medium between the camera and the specimen cause problems with optical DIC.

X-ray imaging can help reduce errors due to beam-steering. X-rays essentially do not refract in air and therefore will not be affected by beam-steering when passing through the optical medium [16–18]. X-rays are also able to penetrate occluding material. The X-ray DIC approach is like optical DIC except visible light illumination is replaced by X-ray machines and optical cameras are replaced by X-ray detectors (consisting of scintillators and optical cameras in this work). The X-rays pass through the object being imaged and create a shadow on the detectors, which represents the attenuation of X-ray photons passing through dense materials. Patterns for X-ray DIC can be developed with differences in densities between pattern features and the surrounding measurement surface. This creates contrast in a manner similar to optical DIC. Another advantage of X-ray DIC is that material can be added to an internal plane in the specimen [19–22]. Viewing internal planes allows access to internal dynamics measurements not possible using optical DIC.

The present work measures the structural dynamics of a beam specimen having internal joints excited by shock-induced flow. As detailed in previous optical DIC measurements [11, 12], the incident shock imparts an impulsive longitudinal force on the beam followed by a transverse forcing associated with periodic vortex shedding. Here, X-ray DIC is performed on an internal surface and directly compared to the previous optical DIC. When optical stereo DIC and X-ray stereo DIC are compared, it is shown that the X-ray measurements have agreement with optical measurements in curve trends and oscillation frequency due to vortex shedding. X-ray measurements also proved to ignore false displacements due to beam-steering.

II. Experimental Arrangement

A. Shock Tube Facility

Experiments were performed in the Multiphase Shock Tube (MST) at Sandia National Laboratories, described in detail in [23] and shown in Fig. 1. Briefly, the MST is a shock tube with a driver section consisting of a circular pipe 89 mm in diameter that is 2.3 m long. The driver was pressurized with air (for optical DIC) or nitrogen (for X-ray DIC) at room temperature. The driven section was a square cross-section pipe of 79 mm height and width, with a length of 5.9 m. It was filled with ambient air at room temperature and atmospheric pressure of 84.1 kPa. The test section was a specialized square section located approximately 4.9 m downstream of the valve. In the X-ray measurements, the thin aluminum "windows" designed to have minimal X-ray attenuation were used. In optical DIC, fused silica windows were used that allowed only the middle 25 mm of the beam to be imaged [12]. The top and bottom portions have solid inserts and provide the mounting points for the specimen.

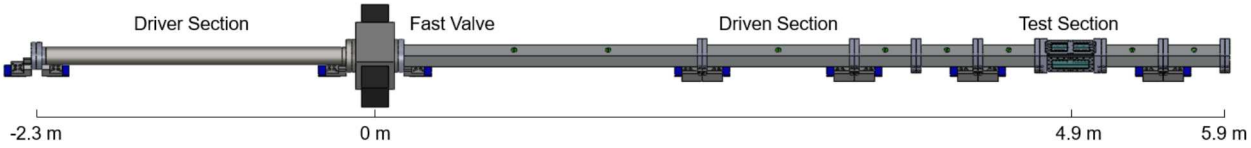

Fig. 1 Diagram of multiphase shock tube with fast-acting valve.

The burst disk diaphragm section has been replaced by a Dynamics Systems Research (model 725-3.0-6000) fast acting valve. The valve was actuated using an independent pressure source, allowing for a continuous range of driver pressure conditions. The continuous range of conditions allows the strength of the structural loading to be widely varied. Further, the valve was electronically triggered to allow for synchronization with X-ray and camera equipment. Similar performances were achieved compared to traditional burst disks [24].

Only one driver pressure, P, was tested in this work, to demonstrate as a proof of concept of X-ray DIC technique. The flow conditions were determined by first measuring the shock speed and Mach number, M_s, near the test section using fast-response pressure transducers. Then shock tube relations were used to calculate the induced velocity, U_∞, and Reynolds number, Re_D, based on specimen width D (Table 1). The values of the vortex shedding frequency, f_{shed}, and the associated Strouhal number, St_D ($f_{shed} \times D / U_\infty$), have been determined by previous pressure sensitive paint (PSP) measurements [11,12]. Five runs each were conducted for the X-ray and optical DIC. In all cases the reflected shock wave arrived prior to the driver gas contact surface.

Table 1. Mean Experimental Conditions

P_4 (psi)	M_s	U_∞ (m/s)	M_∞	q_∞ (kPa)	Re_D	f_{shed} (kHz)	St_D
125	1.42 ± 0.01	206	0.53	44	1.17×10^5	2.86	0.16

B. Test Model

A steel (4340 alloy) specimen with a 12.7 mm × 12.7 mm cross-section was designed to exhibit a nonlinear response when subjected to an impulsive loading and subsequent vortex shedding (Fig. 2). Preliminary finite element analysis (FEA) was used to ensure that a natural frequency of the specimen sensitive to vortex shedding would be active near the anticipated vortex shedding frequencies. The model consisted of a back plate containing two threaded interfaces on raised flanges. These flanges mated to corresponding flanges on a thin 'C-shaped' shell via two bolts. The pressure loading on the faces of the shell is transferred through to the internal bolted joint, causing a localized strain and slip that is nonlinear depending on the input loading. Further, rotation of the shell about this joint can occur under asymmetric loading imposed by vortex shedding.

The back plate of the specimen was connected directly to the shock tube using UNF ¼"-28 bolted connections, torqued to 100 in-lbs. This torque level was verified to be sufficient to prevent measurable slippage of this bolted connection during the experiment. The internal bolts were UNF #3-56, torqued to 8.0 ± 0.5 inch-pounds. The intent was to have the back plate be essentially rigid; however, as discussed in [12], the structural dynamics of the back plate do affect the interaction. The shell piece was 2.5 mm shorter than the back plate, preventing contact between the shell and the shock tube walls, allowing uninhibited movement of the shell.

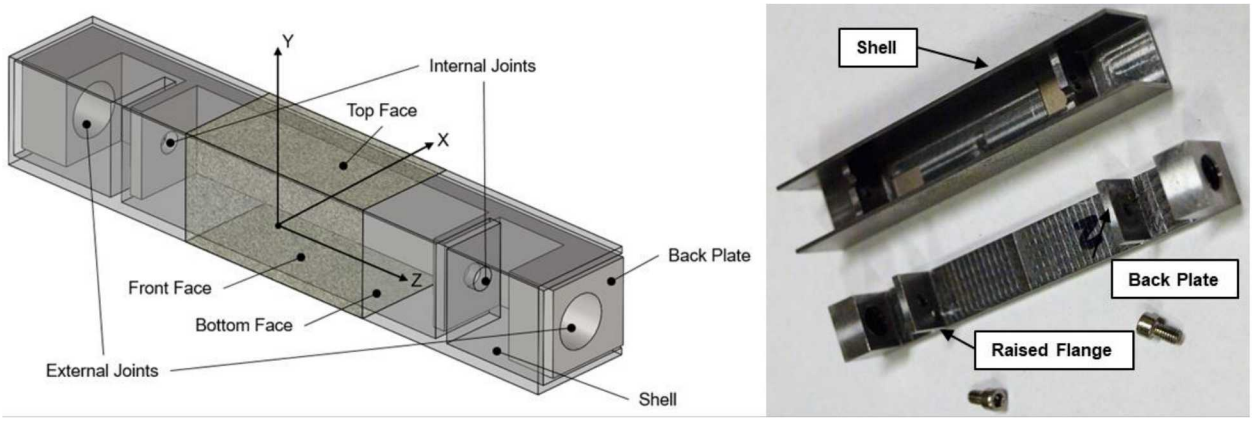

Fig. 2 Model specimen: a) schematic and b) photo showing the specimen disassembled

The full-span specimen assembly was mounted in a vertical orientation within the shock tube; the resulting coordinate system is defined in Fig. 2. The origin is located on the center of the front face of the specimen. Displacements in *x*-direction (*u*) correspond to a response generated from a front face pressure along the streamwise direction, and displacement in the *y*-direction (*v*) correspond to responses from asymmetric pressure loading on the top and bottom face from vortex shedding in the transverse direction. Previous measurements using optical DIC showed that the displacements in the *z*-direction (*w*) in the spanwise direction are minimal since the specimen spans the height of the test section [11, 12]; thus only the *u* and *v* component displacements are shown in this work.

C. Stereo Optical Imaging System

A stereo imaging configuration was used as shown in Fig. 3. Phantom v2512 high speed cameras were used for imaging (28 µm pixels, 1280 x 800 px at 20 kHz). A cropped image size of 256 x 304 was used for this experiment, while the frame rate was maintained at 20 kHz with an exposure time of 49 µs. The total field-of-view was approximately 27 x 32 mm, leading to a physical scaling of the system of ≈ 9.4 px/mm. The field-of-view captured the center 25 mm of the front face of the specimen in both camera systems. Note that viewing of the entire specimen span was precluded by the 25 mm tall test section window. A pair of Nikon AF Nikkor 24-85 mm zoom lenses (set to 85 mm) were used with LaVision Scheimpflug mounts, allowing a low aperture (f/ 2.8) to capture additional signal while aligning the focal plane with the front face of the specimen. The optical DIC setup was originally combined with simultaneous pressure measurements from pressure sensitive paint (PSP) as described in [11, 12]. In the current work, however only the DIC results are discussed.

Illumination is provided by four ISSI LM2XX-DM-460 water-cooled LED arrays, each outputting 12 W at 460 ± 31 nm. The light enters the test section via the same side windows used for imaging. The stereo-angle, defined as the total angle between lenses, was approximately 60° and the stand-off distance was approximately 200 nm. The camera systems were mounted to a large floating vibration isolation table to reduce propagation of shock tube motion through to the cameras.

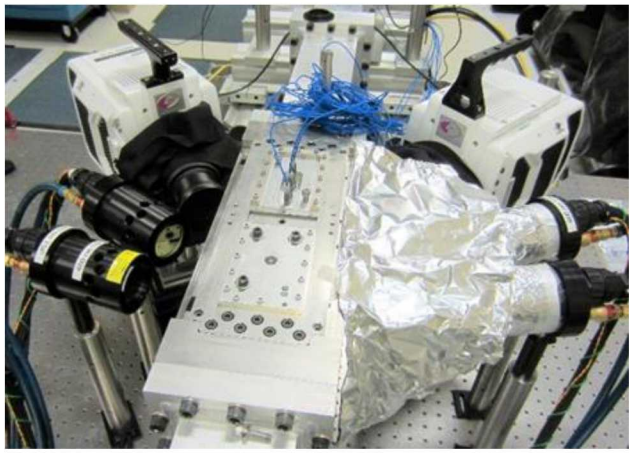

Fig. 3 Stereo optical imaging system.

D. Stereo X-ray Imaging System

The X-ray stereo DIC system is shown in Fig. 4. The same Phantom v2512 cameras as in the optical DIC were used, but with an image resolution of 1280 x 800 px at 10 kHz. The low signal levels in the X-ray DIC precluded a match to the 20 kHz rate in the optical DIC. The cameras captured the entire length of the specimen with a field-of-view of approximately 86 x 54 mm. The cameras were focused on the back of Scintacor Rapidex scintillators with Zeiss Milvus 50 mm lenses with an aperture of f/2. The scintillators converted the X-ray photons to visible light at 513 nm and were positioned 78.7 cm from the X-ray machine and collimator bundle. The distance from the cameras to the scintillators was 10.2 cm. Lead glass panels were placed between the cameras to reduce the amount of higher energy photons saturating the camera. The X-ray machines (Varian G-297 and G-292 tubes both in B-147 housing) operated with an accelerating voltage of 150 keV, a current of 500 mA and a total beam exposure of 250 ms. This exposure time can be considered quasi-continuous in comparison to flash sources having exposures on the order of 10 ns. Note that the exposure time here well exceeds the total test time of the shock tube, which is on the order of 10 ms. Siemens ML03 collimators were coupled to the X-ray machines to narrow the beam profile to the width and length of the specimen and were positioned 29.2 cm from the specimen. The angle of the imaging system with respect to the shock tube was minimized to account for perspective distortions, but geometrical constraints required a stereo angle of approximately 56°. Again, the entire imaging system was mounted on a floating vibration isolation table to eliminate propagation of shock tube motion through to the cameras.

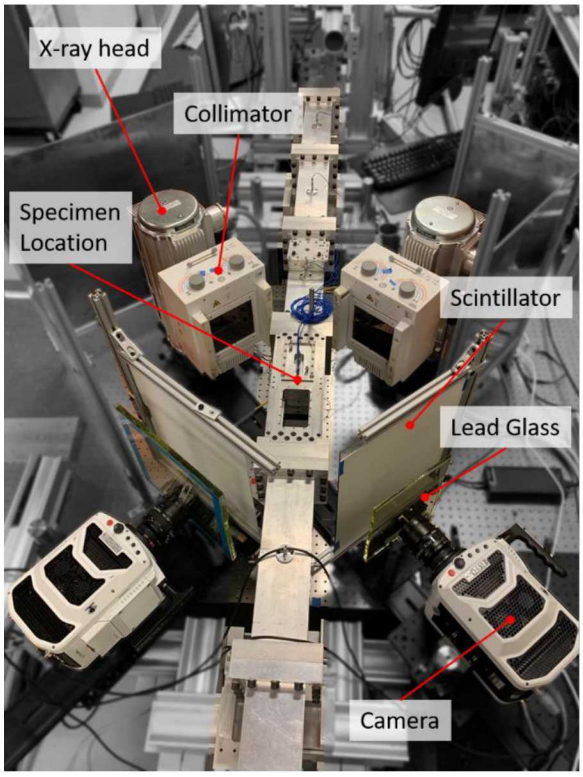

Fig. 4 Stereo X-ray DIC imaging system.

E. Digital Image Correlation

1. *Optical DIC*

Stereo DIC was used to measure the surface deformation of the front face of the specimen. The DIC pattern was created by first applying a layer of PSP (a ruthenium luminiphore ($Ru(dpp)_3$) mixed within a silicone rubber (RTV) binder containing nanoscale boron nitride particles, as described in [11, 12]), and then applying a dot pattern with an ink stamp (Correlated Solutions square ink stamp, 0.013 mm dot size), as shown in Fig. 5. The thin layer of ink effectively blocks the UV excitation light from reaching the lumiphores and results in a high-contrast pattern. A sparse speckle pattern was used as a compromise between the optimal speckle density for DIC and maintaining sufficient PSP paint uncovered. In 16-bit quantization, the minimum intensity within the speckles is around 1900 counts, the maximum intensity is around 14000 counts, and the image noise level, defined here as standard deviation of the background, is 260 counts. This yields a contrast, defined here as (14000-1900) / 260 = 50, which was found to be sufficient for DIC processing.

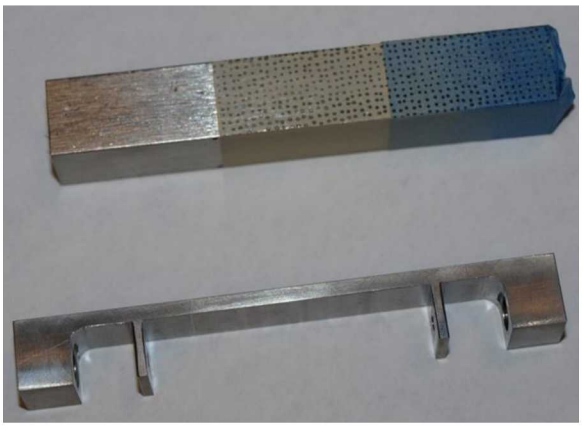

Fig. 5 Applied PSP and speckle pattern on specimen.

Correlated Solutions VIC-3D v8 software was used for calibration and evaluation. Two sets of calibration images were collected, one using a standard dot-grid calibration target and a second using a speckled flat plate that filled the field of view. Approximately 100-200 images were captured of each target as the target was rotated, tilted, and plunged within the field-of-view and depth-of-field of the two optical systems. To mitigate distortions caused by imaging through the thick windows at a glancing angle, a hybrid calibration was performed using both sets of calibration images, with a 5^{th} order variable ray origin camera model, as described in [11, 12].

Processing used a subset size of 35 pixels, a step size of 10 pixels and an affine subset shape function. Because the specimen motion during the experiment had low spatial gradients, a large subset size was used to reduce noise, and a large step size was used to reduce processing time over 6000 images. To account for the variation in image intensity between the reference and 'wind-on' (i.e., during shock tube experiment) images, it was required to use a zero-mean normalized cross-correlation. A low-pass filter was applied to the images prior to correlation.

2. *X-ray DIC*

A speckle pattern for X-ray DIC was generated by hand-dotting a mixture of Tantalum and epoxy (1.1:11 wt. ratio) on the inside of the front shell shown in Fig. 6. The X-ray mass attenuation coefficient for tantalum is about 6 times greater than that of steel over the x-ray spectrum (20-150 keV) [25, 26] . The high mass attenuation coefficient of tantalum gives the contrast needed with the steel to perform X-ray DIC. The X-ray images were normalized with a static light-field image sequence where no specimen was in the beam path. The light-field images were then averaged and all specimen images were corrected by dividing by the averaged light field images. After light-field correction and histogram equalization, the minimum intensity of the speckles was 0 and the maximum intensity was 38,337 on a 16-bit scale. The minimum intensity of the steel specimen was 8794 and the maximum intensity was 65535.

Calibration images were collected using a standard dot-grid calibration target. The calibration target was fabricated using printed circuit-board processes, where gold dots of 2.5 mm diameter were etched in a 9 x 9 array with 5 mm spacing on the printed circuit board substrate. The X-ray machines were adjusted to 50 keV, 500 mA, and 640 ms beam exposure while the cameras were adjusted to 100 Hz frame-rate and 9900 µs exposure to improve contrast between the calibration target dots and the background. To further improve calibration image quality, the aluminum windows on the shock tube were removed. Due to the onerous nature of collecting X-ray images, only 16 different positions were captured, as the target was rotated, tilted, and plunged within the measurement volume; in the future, remote-controlled, motorized stages would allow the efficient capture of more calibration images. The image sequences at all positions were light-field corrected and time averaged.

Correlated Solutions VIC-3D v8 was used to calculate displacements. A subset size of 71 pixels and a step size of 11 pixels were used. The large subset was required because the tantalum/epoxy dots were approximately 40 pixels in diameter. In the future, the pattern should be optimized to achieve features closer to 3-5 px, as described by the *Good Practice Guide for Digital Image Correlation* [14]. However, as with the optical DIC, because the primary motion of

interest was rigid-body motion, the large subset size was acceptable. The VIC-3D internal low pass filter was applied to all images. The gaussian weights subset weight option was used, and the criterion was zero-normalized squared differences. A reference image was created by taking static images of the specimen and averaging the image sequence.

Note that the patterned surface is not optically visible when the specimen is assembled, and thus would be impossible to measure directly with standard optical-DIC. However, it is reasonable to assume as a first-order approximation that the outside and inside surfaces on the front face of the shell both experience the same motion/deformation. Therefore, by patterning the inside surface, we accomplish two goals simultaneously: (1) X-ray DIC measurements are demonstrated on a surface that is not optically visible, and (2) X-ray DIC measurements can be directly compared with optical DIC measurements made previously [12].

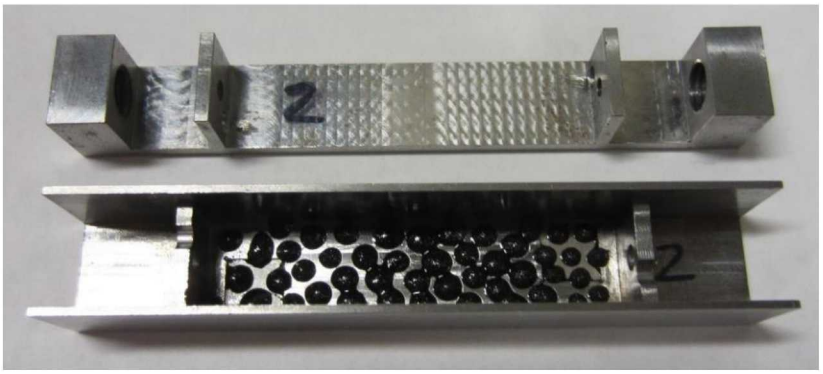

Fig. 6 Front shell of specimen with hand dotted Ta-epoxy mixture speckle pattern.

III. Results and Discussion

IV. A complete evaluation of image quality – namely noise and contrast – is currently underway, but visual inspection of the images shows that the X-ray images are noticeably noisier than optical images. This leads to a low signal-to-noise ratio for the X-ray images. As a result, the correlation from the X-ray data is poorer than the correlation from the optical data, as shown by the "holes", or places where the correlation failed, in the contour plots for streamwise full-field displacement (Fig. 7). VIC-3D is able to correlate 23% of the X-ray ROI while 47% is correlated for the optical ROI. In Fig. 7, the correlated regions of both measurement types can be seen by the colored contours. Failed regions are the perimeter around the contour as well as holes in the contour region for the X-ray case. Additionally, for a few, random images within the series, significant portions of the region of interest failed to correlate. Similar considerations attend the transverse displacements. Because the primary structural displacements of interest were rigid-body-motion, the displacements in the region of interest, outlined by the boxes in Fig. 7, were spatially averaged at each point in time, collapsing the full-field data to 1D displacement versus time curves. This allowed a direct comparison between the two DIC measurement techniques. For all displacement versus time curves, $t = 0$ is the time the incident shock arrives at the front face of the beam.

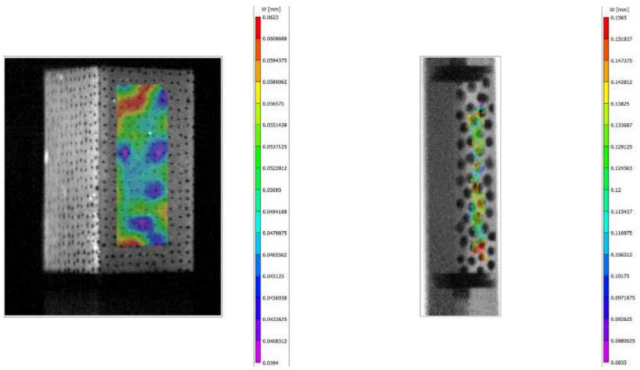

Fig. 7 Streamwise displacement contour for (left) optical stereo DIC and (right) X-ray stereo DIC at t = 0.

The shock tube has a high amplitude, low frequency motion caused by the recoil of the entire shock tube on a millimeter length scale. DIC measurements of the beam surface are a convolution of the beam motion and the shock tube recoil, as seen in Fig. 8. A polynomial fit was applied to the DIC data to detrend this shock tube motion. Optical

data used a 13th order polynomial for both the streamwise and transverse displacements. X-ray data used a 11th order polynomial for transverse and a 5th order polynomial for streamwise displacements. Time ranges were selected to capture sufficient shock tube motion for the polynomial fit. Times ranging from -3 – 35 ms for X-ray and -5 – 60 ms for optical were used. Since the polynomial was intended to model only the shock tube recoil, it was necessary to mask regions of the displacement curves dominated by the beam motion, so that the beam motion did not influence the polynomial fit. For the transverse displacements, no mask was necessary, since the transverse beam motion was periodic and centered about the shock tube motion. For the streamwise displacements, a mask from -0.25 to 15 ms was selected for both the optical and X-ray displacements. It was found that the data is sensitive to this detrending process as selection of the total time range, masking region, and polynomial order can output various detrended curves. Work continues to develop a more robust and less sensitive detrending process.

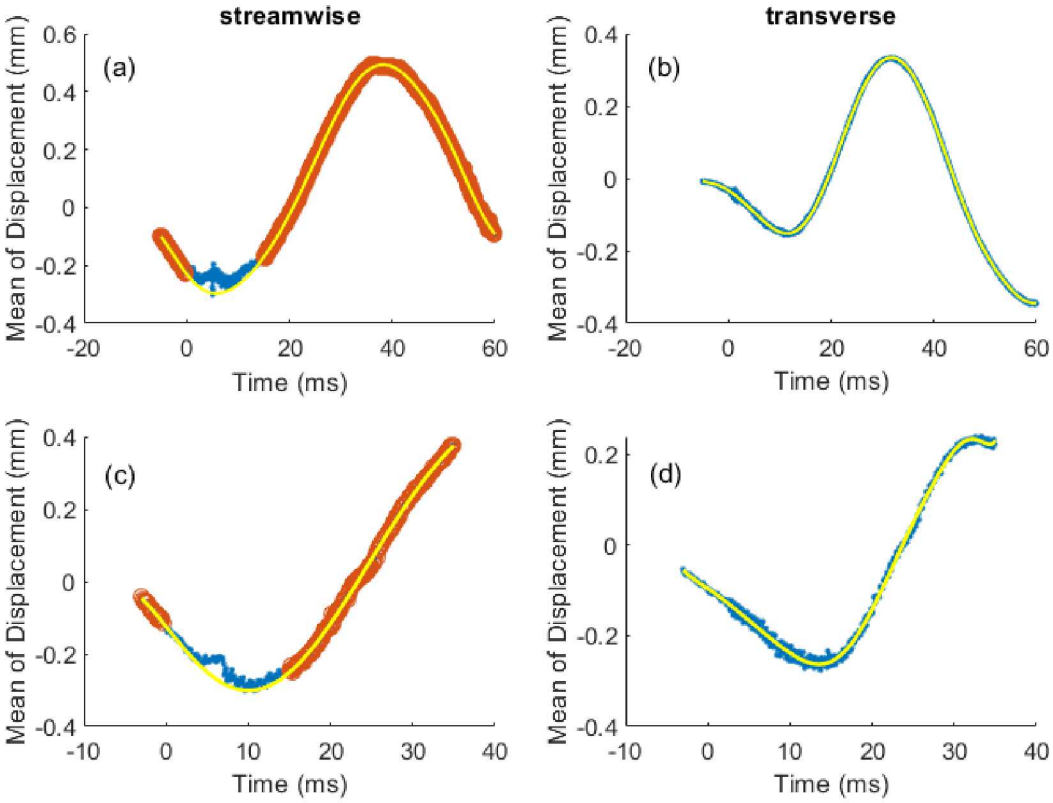

Fig. 8 Detrending curves. Blue curves are the DIC data, and yellow curves are the polynomial fit. Orange circles indicate the portion of the data used for the polynomial fit. a and b are optical data. c and d are X-ray data.

To compute the noise floor of the DIC displacement data, the same detrending process was done on a time interval ranging from -35 to -8 ms for the optical case and -21 to -8 ms for the X-ray case. After detrending, the standard deviation in time was calculated and is tabulated in Table 2. The X-ray measurements are approximately two times noisier than the optical measurements, which is consistent with the qualitative observations of image noise made previously. Possible sources of noise in the X-ray images and X-ray DIC measurements include camera noise, scintillator defects or blemishes, the rotating anode of the X-ray machines, and poor contrast in the DIC pattern. Noise in the X-ray displacements can be improved in part by optimizing the speckle size as well as improving speckle application to ensure that speckles are a consistent thickness and size. This will improve contrast and thus improve image quality.

Table 2. Noise floor in µm using data before arrival of incident shock

	Optical		X-ray	
	u	***v***	***u***	***v***
1	1.03	0.67	1.62	1.41
2	1.05	0.71	2.14	1.94
3	1.22	0.79	2.49	2.03
4	1.44	0.98	1.76	1.45
5	0.81	0.57	2.32	2.19
Average	1.11	0.74	2.06	1.80

The specimen exhibits several modes as it is excited by the impulsive force of the shock wave and subsequent shock-induced flow [12]. Two main modes that will be investigated here are a streamwise translational mode due to the impulsive force of the incident shock wave followed by a rocking mode due to transverse loading imposed by asymmetric vortex shedding. To visualize the two main modes, comprise approximately 60% of the total energy, a proper orthogonal decomposition (POD) was used and is shown in Fig. 9. This POD visualization was created using the optical DIC results as described in Lynch et al. [12]. The first POD mode represents a streamwise translation of the beam in the *x*-direction, characterized by the *u*-displacement as shown in Fig. 9a. The second POD mode is a rocking mode, where the face of the beam rotates along its central axis, causing a pronounced *v*-component displacement as shown in Fig. 9b. These modes can be further characterized by their temporal frequency as the specimen is undergoing the interaction. Using an impact hammer test, the rocking frequency was experimentally determined to be between 2480-2720 Hz and the streamwise translating mode was 2810 Hz [12].

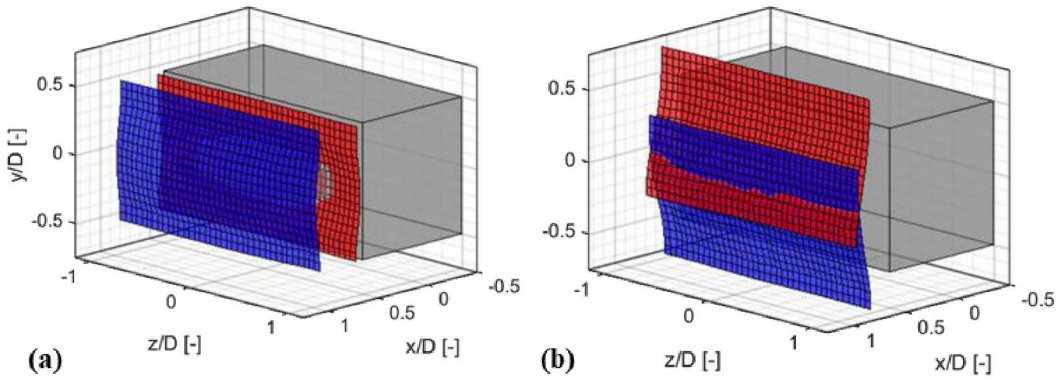

Fig. 9 POD modes of beam displacement: a) streamwise translation and b) vertical rocking. Reproduced from Lynch et al. [12].

The optical streamwise and transverse displacements, representing respectively the streamwise translation and rocking modes, for all runs can be seen in Fig. 10. The detrending process is successful in removing the shock tube motion while maintaining specimen motion. The dashed vertical lines represent incident and reflected shock arrival times at the front face of the beam. Aero-optical distortions associated with shock waves, turbulence, and shock-heated gas contribute to measurement noise and bias in the optical DIC measurements. The incident and reflected shock waves are the most dominate and are followed by increase in fluid density proportional to the shock strength, leading to a change in the refractive index of the air described by the Gladstone-Dale relation [27]. The streamwise displacement shows distortions caused by refraction indicated by the rapid rise before the incident shock arrival and the rapid decrease and rise near the reflected shock arrival. Due to the camera orientation, the shock fronts do not affect the transverse displacements [28] The specimen motion can also be seen by the oscillations in both the streamwise and transverse directions. In particular, the transverse displacements characterize the rocking motion about the interior joint in response to the vortex shedding. It takes about 1.0 ms for the transverse oscillations to peak owing to the impulsive start of the cylinder wake [12]. Over 5 runs, streamwise displacement curves remain consistent and follow the same trends as well as mostly maintaining amplitude and frequency of the oscillations. On the other hand, transverse displacement curves remain consistent between 0 and 1.5 ms but consistency is lost at later times. The run-to-run variation in the transverse amplitudes is suspected to be related to the sensitive nature of the dynamics of the jointed structure rather than measurement error.

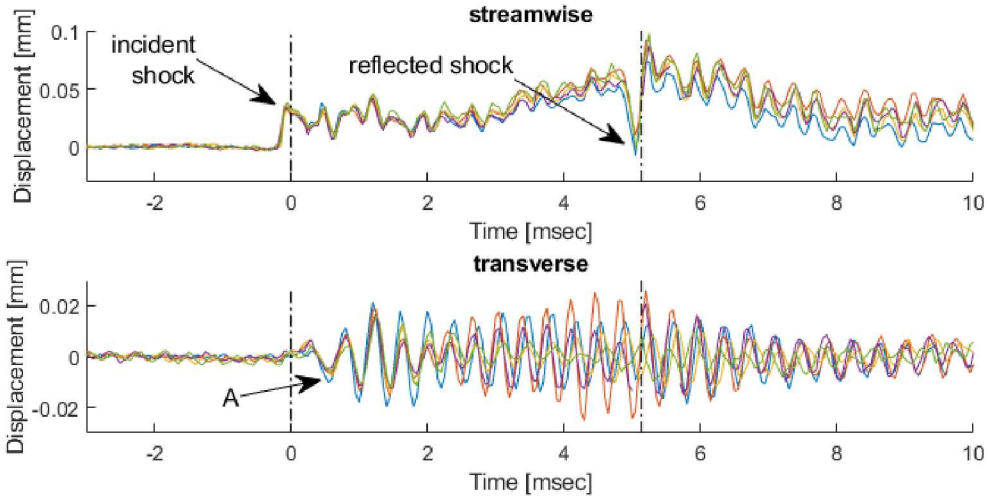

Fig. 10 Detrended optical displacements for 5 runs. The dashed line at t = 0 is the incident shock arrival at the front face of the beam. The second dashed line is the reflected shock arrival at the front face of the beam.

There is significant jitter in the triggering of the X-ray sources and cameras with respect to the shock tube. To compensate, the X-ray data for each run was time shifted so that the first valley in the transverse displacements was aligned with the first valley in the optical transverse displacements (labeled "A" in Fig. 10-Fig. ***11***). The time shifted X-ray displacements for all runs can be seen in Fig. 11. The rocking motion of the specimen can be seen by the oscillations in the transverse direction. These oscillations are similar to those observed with optical DIC, shown in Fig. 10. Recall that the X-ray images were captured at 10 kHz while the optical images were captured at 20 kHz; thus, the oscillations in the optical data are resolved more clearly. The oscillations for the streamwise displacement are less obvious in the X-ray data. This is in part due to the lower sampling rate and higher noise. Similar to the optical measurements, repeatability between the five runs is good for the streamwise displacements and for the transverse displacements from 0-2 ms, with larger variability exhibited in the transverse displacements at later times.

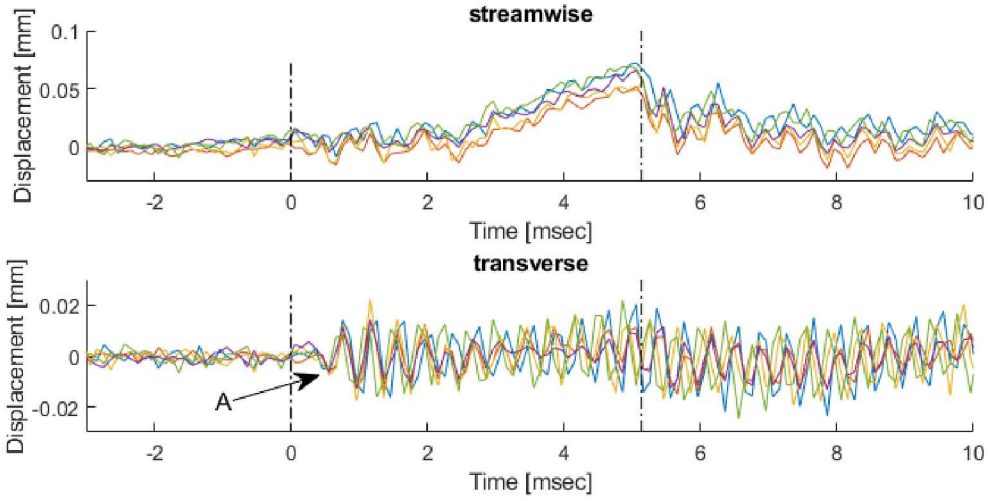

Fig. 11 Detrended X-ray displacements for 5 runs. The dashed line at t = 0 is the incident shock arrival at the front face of the beam. The second dashed line is the reflected shock arrival at the front face of the beam.

With the time shifted X-ray data, the two measurement techniques are now compared by averaging all five runs as shown in Fig. 12. Overall, the X-ray data follows similar trends as the optical data. For the streamwise component, the beam front face moves in the positive x-direction as a result of the incident shock and the post-shock flow. The rate of motion (slope of the curves) is approximately the same for both the optical and X-ray measurements. Displacements then return to the initial position at the same rate as the reflected shock moves back through the shock tube. For the transverse component, X-ray stereo DIC was able to capture the same transverse rocking motion of the

specimen with similar amplitude and frequency between t = 0 and t = 3.5 ms. Notably, the main difference between the X-ray and optical data is the incident and reflected shock indications, which are present in the optical streamwise data and absent in the X-ray data. Again, these indications are the rapid rise before the incident shock arrival and the rapid decrease and rise near the reflected shock arrival as labeled in the figure. The X-ray data is showing true beam motion unaffected by refraction due to the density gradients from the shock waves as they propagate through the shock tube. The error bar are student t 95% confidence intervals.

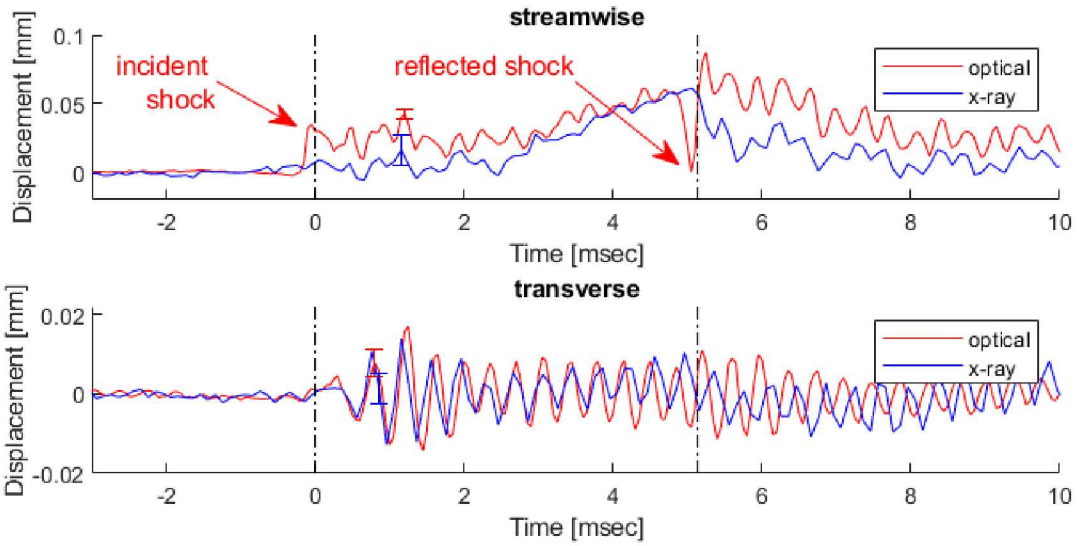

Fig. 12 Mean of 5 runs for optical and X-ray displacements. The error bars are 95% confidence intervals based on student-t theory.

A comparison of power spectral densities (PSDs) for the streamwise and transverse displacement is shown in Fig. 13. Each PSD is computed in an identical fashion using the Welch windowing algorithm (*pwelch* function) in MATLAB. The rocking motion frequency is matched between both measurement types at 2700 Hz. This frequency corresponds to the combination of the vortex shedding and a match to the rocking natural frequency. The rocking frequency was experimentally measured via impact hammer to be between 2480-2720 Hz [12]. For the streamwise component, the peaks match around 2800 Hz which corresponds to the bending-translating natural frequency (experimentally determined to be 2810 Hz). Importantly, both the optical and X-ray DIC results give statistically identical peak amplitudes, highlighting the viability of the X-ray DIC technique to be used on internal surfaces as well as overcome aero-optical distortions associated with shock waves.

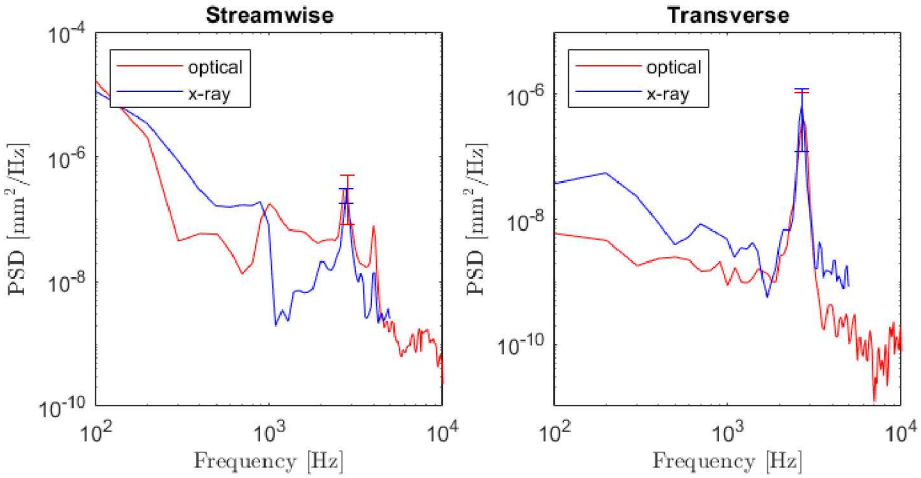

Fig. 13 PSDs for streamwise and transverse displacements

Conclusion

X-ray stereo digital image correlation (DIC) measurements were performed at 10 kHz on a jointed structure in a shock tube at a shock Mach number of 1.42. The X-ray measurements were compared to optical DIC measurements made at 20 kHz on the same structure in the same shock tube flow. Displacement time traces for the averaged full-field data were in good agreement over the time period between the incident and reflected shock arrival times. Structural oscillations peaked at identical frequencies, and the streamwise translations had similar low frequency behaviors associated with shock arrival. Both measurement systems were able to capture the primary structural dynamics of the beam in the shock-induced flow. The advantage of using optical DIC is the increased signal-to-noise ratio for better correlations, which provide full-field data. X-ray DIC image quality can be improved by speckle pattern optimization and contrast to allow for the full-field displacement comparison. In comparison to optical DIC, the key advantages of the X-ray DIC demonstrated herein are: (1) the ability to perform DIC measurements on the internal surface of a structure, and (2) the potential to remove bias errors associated with aero-optical refraction.

Acknowledgements

The authors wish to acknowledge Paul Farias, Tom Grasser, Seth Spitzer and Anthony McMaster for assistance in setting up and conducting the experiments. This work was supported by the Laboratory Directed Research and Development (LDRD) program at Sandia National Laboratories. Sandia National Laboratories is a multimission laboratory managed and operated by National Technology & Engineering Solutions of Sandia, LLC, a wholly owned subsidiary of Honeywell International Inc., for the U.S. Department of Energy's National Nuclear Security Administration under contract DE-NA0003525. This paper describes objective technical results and analysis. Any subjective views or opinions that might be expressed in the paper do not necessarily represent the views of the U.S. Department of Energy or the United States Government

References

[1] Wagner, J. L., Casper, K. M., Beresh, S. J., Hunter, P. S., Spillers, R. W., and Henfling, J. F. "Response of a Store with Tunable Natural Frequencies in Compressible Cavity Flow." *AIAA Journal*, Vol. 54, No. 8, 2016, pp. 2351–2360. doi:10.2514/1.J054688.

[2] Blackman, D. R., Clark, D. M., McNulty, G. J., and Wilby, J. F. "Boundary Layer Pressure Fluctuations and Structural Response." *Technical Report AFFDL-TR-67-97, Air Force Flight Dynamics Laboratory*, 1967.

[3] Casper, K. M., Beresh, S. J., Henfling, J. F., Spillers, R. W., Hunter, P. S., and Spitzer, S. M. "Hypersonic Fluid-Structure Interactions on a Slender Cone." *AIAA Paper 2018-1825*, 2018. doi:10.2514/6.2018-1825.

[4] Currao, G. M. D., Neely, A. J., Buttsworth, D. R., and Choudhury, R. "Measurement and Simulation of Hypersonic Fluid-Structural Interaction on a Cantilevered Plate in a Mach 6 Flow." *AIAA Paper 2016-1088*, 2016. doi:10.2514/6.2016-1088.

[5] Maestrello, L., and Linden, T. L. J. "Measurements of the Response of a Panel Excited by Shock Boundary-Layer Interaction." *Journal of Sound and Vibration*, Vol. 16, No. 3, 1971, pp. 385–391.

[6] Willems, S., Gulhan, A., and Esser, B. "Shock Induced Fluid-Structure Interaction on a Flexible Wall in Supersonic Turbulent Flow." *Progress in Flight Physics*, Vol. 5, 2013, pp. 285–308. doi:10.1051/eucass/201305.

[7] Perez, R., Bartram, G., Beberniss, T., Wiebe, R., and Spottswood, S. M. "Calibration of Aero-Structural Reduced Order Models Using Full-Field Experimental Measurements." *Mechanical Systems and Signal Processing*, Vol. 86, 2017, pp. 49–65. doi:10.1016/j.ymssp.2016.04.013.

[8] Maestrello, L. "Control of Shock Loading from a Jet in a Flexible Structure's Presence." *AIAA Journal*, Vol. 38, No. 6, 2000, pp. 972–977. doi:10.2514/2.1080.

[9] Hortensius, R., Dutton, J. C., and Elliott, G. S. "Simultaneous Planar PIV and SDIC Measurements of an Axisymmetric Jet Flowing Across a Compliant Surface." *AIAA Paper 2017-1886*, 2017. doi:10.2514/6.2017-1886.

[10] Dowell, E. H. "Panel Flutter-A Review of the Aeroelastic Stability of Plates and Shells." *AIAA Journal*, Vol. 8, No. 3, 1970, pp. 385–399. doi:10.2514/3.5680.

[11] Lynch, K. P., Jones, E. M., and Wagner, J. L. "Simultaneous PSP and DIC Measurements for Fluid-Structure Interactions in a Shock Tube." *AIAA Paper 2018-3870*, 2018. doi:10.2514/6.2018-3870.

[12] Lynch, K. P., Jones, E. M., Brink, A. R., Roettgen, D. R., Kuether, R. J., Wagner, J. L., Mathis, A., and Quinn, D. D. "Response of Jointed-Structures in a Shock Tube : Simultaneous PSP and DIC with Comparison to Modeling." *AIAA Paper 2019-3654*, 2019.

[13] Sutton, M. A., Orteu, J.-J., and Schreier, H. *Image Correlation for Shape, Motion, and Deformation Measurements: Basic Concepts, Theory and Applications*. Springer Science & Business Media, 2009.

[14] Jones, E. M. C., and Iadicola, M. A., Eds. *A Good Practices Guide for Digital Image Correlation*. International Digital Image Correlation Society, 2018.

[15] Jones, E. M. C., and Reu, P. L. "Distortion of Digital Image Correlation (DIC) Displacements and Strains from Heat Waves." *Experimental Mechanics*, Vol. 58, No. 7, 2018, pp. 1133–1156. doi:10.1007/s11340-017-0354-3.

[16] Henke, Burton L., Gullikson, E. M., and Davis, J. C. X-Ray-Interactions--Photoabsorption--Scattering--Transmission--

and-Reflection-at-E---50-30-000-EV--Z---1-92_1993_Atomic-Data-and-Nuclear-Data-Tables.
[17] Thompson, A., Attwood, D., Gullikson, E., Howells, M., Kim, K.-J., Kirz, J., Kortright, J., Lindau, I., Liu, Y., Pianetta, P., Robinson, A., Scofield, J., Underwood, J., Williams, G., and Winick, H. X-Ray Data Booklet. *Lawrence Berkeley National Laboratory*.
[18] Chantle, C. T., Olsen, K., Dragoset, R. A., Chang, J., Kishore, A. R., Kotochigova, S. A., and Zucker, D. S. X-Ray Form Factor, Attenuation, and Scattering Tables. *NIST Standard Reference Database 66*.
[19] Russell, S. S., and Sutton, M. A. "Strain-Field Analysis Acquired through Correlation of X-Ray Radiographs of a Fiber-Reinforced Composite Laminate." *Experimental Mechanics*, Vol. 29, No. 2, 1989, pp. 237–240. doi:10.1007/BF02321382.
[20] Synnergren, P., Goldrein, H. T., and Proud, W. G. "Application of Digital Speckle Photography to Flash X-Ray Studies of Internal Deformation Fields in Impact Experiments." *Applied Optics*, Vol. 38, No. 19, 1999, pp. 4030–4036. doi:10.1364/ao.38.004030.
[21] Prentice, H. J., Proud, W. G., Walley, S. M., and Field, J. E. "The Use of Digital Speckle Radiography to Study the Ballistic Deformation of a Polymer Bonded Sugar (an Explosive Simulant)." *International Journal of Impact Engineering*, Vol. 37, No. 11, 2010, pp. 1113–1120. doi:10.1016/j.ijimpeng.2010.05.003.
[22] Synnergren, P., and Goldrein, H. T. "Dynamic Measurements of Internal Three-Dimensional Displacement Fields with Digital Speckle Photography and Flash x-Ray." *Applied Optics*, Vol. 38, No. 28, 1999, pp. 5956–5961.
[23] Wagner, J. L., Beresh, S. J., Kearney, S. P., Trott, W. M., Castaneda, J. N., Pruett, B. O., and Baer, M. R. "A Multiphase Shock Tube for Shock Wave Interactions with Dense Particle Fields." *Experiments in Fluids*, Vol. 52, No. 6, 2012, pp. 1507–1517. doi:10.1007/s00348-012-1272-x.
[24] Wagner, J. L., Beresh, S. J., Demauro, E. P., Casper, K. M., Guildenbecher, D. R., Pruett, B., and Farias, P. "Pulse-Burst PIV of an Impulsively Started Cylinder in a Shock Tube for Re> 10 5." *Experiments in Fluids*, Vol. 59, No. 6, 2018, p. 106. doi:10.2514/6.2016-0791.
[25] Hubbel, J. H., and Seltzer, S. M. X-Ray Mass Attenuation Coefficients. *NIST Standard Reference Database 126*.
[26] Berger, M. J., Hubbell, J. H., Seltzer, S. M., Chang, J., Coursey, J. S., Sukumar, R., Zucker, D. S., and Olsen, K. XCOM: Photon Cross Sections Database. *NIST Standard Reference Database 8 (XGAM)*.
[27] Merzkirch, W. *Flow Visualization*. Elsevier, 2012.
[28] Lynch, K. P., Jones, E. M. C., and Wagner, J. L. "High-Precision Digital Image Correlation for Fluid-Structure INteractions in a Shock Tube." *submitted to Experimental Techniques*, 2019.